Composites of Carbon Nanofibers and Thermoplastic Polyurethanes With Shape-Memory Properties Prepared by Chaotic Mixing

Guillermo A. Jimenez,[1] **Sadhan C. Jana**[2]
[1] *Laboratory of Polymers (POLIUNA), School of Chemistry, Universidad Nacional, Heredia, Costa Rica*

[2] *Department of Polymer Engineering, University of Akron, Akron, Ohio 44325*

Composites of carbon nanofibers (CNFs), oxidized carbon nanofibers (ox-CNFs), and shape-memory thermoplastic polyurethane (TPU) were prepared in a chaotic mixer and their shape-memory properties evaluated. The polymer was synthesized from 4,4′-diphenylmethane diisocyanate, 1,4-butanediol chain extender, and semicrystalline poly(ε-caprolactone) diol soft segments. The shape-memory action was triggered by both conductive and resistive heating. It was found that soft segment crystallinity and mechanical reinforcement by nanofibers produced competing effects on shape-memory properties. A large reduction in soft segment crystallinity in the presence of CNF and stronger mechanical reinforcement by well-dispersed ox-CNF determined the shape-memory properties of the respective composites. It was found that the maximum shape recovery force, respectively, 3 and 4 MPa, was obtained in the cases of 5 and 1 wt% CNF and ox-CNF, respectively, compared with ~1.8 MPa for unfilled TPU. The degree of soft segment and hard segment phase separation and thermal stability of the composites were analyzed. POLYM. ENG. SCI., 49:2020–2030, 2009.

INTRODUCTION

Thermoplastic polyurethanes (TPUs) are versatile materials; their chemistry, structure, and morphology are often tweaked to obtain desired final properties. TPUs are synthesized by one- and two-step processes from diisocyanates, such as 4,4′-diphenylmethane diisocyanate (MDI), linear polyether or polyester diols, and chain-extending diols, such as 1,4-butanediol (BDO) [1]. The reactions between isocyanates and diols are often catalyzed by acids, bases, e.g., aliphatic tertiary amines, and metal complexes, e.g., organotin compounds [1].

TPUs offer high elongation, moderate tensile strength and Young's modulus, and excellent abrasion and tear resistances. These complementary properties originate from microphase separation of the hard and soft segments [2]. The microphase separated TPUs exhibit interconnecting networks [3] with short-range, ordered hydrogen bonding between hard and soft segments [4] or lamellar hard segments with average separation of 100–250 Å acting as crosslinks [5]. The phase separated hard segments inhibit stress relaxation, induce stress crystallization of the soft segments, and are stabilized via interurethane hydrogen bonds [6, 7]. These morphological building blocks play profound roles in shape-memory performance of polyurethanes.

Shape-memory polymers (SMPs) change shape when an external stimulus, such as heat, electrical voltage, pH and moisture change, and light is applied [8–11]. In the first step in a typical shape-memory cycle, the polymer is given a permanent shape by film extrusion, fiber spinning, injection molding, etc. The polymer is then deformed by bending, extension, or compression, and the temporary shape is fixed by cooling usually to room temperature. The original shape is recovered when stimuli, such as heat or electricity, are applied. First shape-memory polymer in the form of polyurethane foams was reported in patent literature in 1966 [12]. Shape-memory polyurethane foams with 40 different compositions of diisocyanates, polyol, chain extenders, and blowing agent were reported in a US patent [13]. In the same manner, Hayashi et al. [14, 15] invented urethane-based transparent shape-memory films for packaging applications. These findings were later summarized in research publications by Hayashi in 1993 [16] and by Hayashi et al. in 1995 [17]. Systematic studies on segmented polyurethanes with shape-memory behavior appeared later [18–26]. It was elaborated that the hard segments act as crosslinks and are responsible for the

Correspondence to: Sadhan C. Jana; e-mail: janas@uakron.edu
Contract grant sponsors: National Science Foundation Faculty Early Career Program, The Fulbright Commission of the Department of State, USA, the Laboratory of Polymers. (POLIUNA) of the Universidad Nacional of Costa Rica, The Science and Technology Bureaus of Costa Rica (MICIT and CONICIT).
DOI 10.1002/pen.21442
Published online in Wiley InterScience (www.interscience.wiley.com).

permanent shape of the articles. The soft segments, on the other hand, serve as molecular switch and are responsible for shape recovery from temporary, deformed shapes. The transition temperature for shape recovery can be either the glass transition temperature, T_g, or the melting temperature, T_m. Several soft segments for T_g-controlled shape recovery have been studied, such as poly(tetramethylene oxide) glycol [23, 24], poly(ethylene adipate) glycol [20], and poly(tetrahydrofuran) [8]. The soft segments to provide T_m-controlled shape-memory behavior are mostly based on poly(ε-caprolactone) diol (PCL-diol) [19, 21, 26–31]. The most common TPU system studied to date is synthesized from PCL-diol, MDI, and BDO in which PCL-diols with number-average molecular weight (M_n) between 2000 and 8000 form the switching segments. The switching temperature for the shape-memory effect ranges between 44 and 55°C as the soft segment content is varied between 50 and 90 wt%. The crystallization of segments of PCL-diol in TPU is restricted because of the connectivity between the soft and the hard segment phases. In most cases, the PCL-diol crystallinity in TPUs varies between 10 and 40% compared with 100% for PCL-diol itself [21].

The shape-memory properties of composites of TPU synthesized from MDI, BDO, and PCL-diol and carbon black (CB) were studied by Li et al. [32]. These authors observed a reduction in soft segment crystallinity for up to 10 wt% CB. The electrical conductivity and storage modulus increased significantly at 20 wt% CB loading because of formation of continuous networks by CB particles, although a large reduction in recoverable strain was also observed. Vaia and coworkers [33, 34] obtained higher shape recovery force than pristine TPU in composites of TPU and 5 wt% multiwall carbon nanotubes (MWNT) and in TPU filled with 20 wt% CB. An increase in soft segment crystallinity in the presence of MWNT contributed to higher shape recovery force, although Cao and Jana [28] and Gunes et al. [30] reported reduction of PCL-diol crystallinity in the presence of nanoscale-dispersed organically modified reactive clay and nanometer-size silicon carbide particles. Paik et al. [35] reported increase of electrical resistance upon elongation of composites of shape-memory TPU and CB and CNT. Cho and coworkers [36, 37] were able to actuate shape-memory action in nanocomposites of TPU/MWNT by resistive heating.

In this work, carbon nanofibers—untreated (CNF) and oxidized (ox-CNF)—were used to prepare composites of PCL-diol-based shape-memory TPU. The composites were prepared by bulk polymerization in a chaotic mixer. The study particularly investigated the following questions. First, it was not apparent if improvements in shape recovery force observed in previous work with MWNT [32–37] can also be obtained with CNF and ox-CNF. This is especially interesting as CNF and ox-CNF are available from manufacturers as agglomerates. It is known that agglomerates are difficult to disperse and efforts to disperse them well often lead to breakage and attrition. Most prior work on MWNT/TPU composites [32–37] reported excellent dispersion of carbon nanotubes. The chaotic mixer was used to exploit its low shear nature. Second, it was expected that ox-CNF would disperse better than CNF fibers because of the presence of polar functional groups on them. However, it was not readily apparent how the shape-memory properties would be affected by the polar functional groups on ox-CNF. Third, CNFs are intrinsically less electrically conductive than CNTs. The magnitude of electrical conductivity of the composites and the possibility of shape memory actuation by resistive heating remained unexplored, especially in light of low shear dispersion in chaotic mixer and anticipated reduction of PCL-diol crystallinity in the presence of CNF and ox-CNF.

EXPERIMENTAL

Materials

PCL-diol, grade CAPA® 2403D from Solvay (Bruxelles, Belgium) with melting temperature range 55–60°C and weight-average molecular weight 4000 was used as soft segment. The hard segment was based on 4,4′-diphenylmethane diisocyanate (MONDUR M® flakes, Bayer, Pittsburgh, PA) and 1,4-butanediol (Avocado, Ward Hill, MA) as chain extender. Dibutyltin dilaurate DABCO 120® from Air Products (Allentown, PA) was used as the catalyst for chain extension reactions. The material contained 33 wt% hard segment. Carbon nanofiber and oxidized carbon nanofiber grades PR-24-PS and PR-24-PS-OX were provided by Applied Sciences (Cedarville, OH) both with a density of 1.95 g/mL, fiber diameters around 200 nm, and average length around 65 μm. ox-CNFs were obtained by air oxidation of CNF at 400–500°C [38], although a detailed account of the surface treatment was not disclosed by the supplier.

Composite Preparation

TPU was synthesized by a two-step polymerization procedure. MDI and polyol were reacted in 2:1 molar ratio in a three-neck round bottom glass reactor at 80°C for 2.5 h with mechanical stirring to produce the prepolymer. In a second step, 80 g of molten prepolymer was hand-mixed with proper amounts of CNF or ox-CNF followed by mixing with 6.5 g of BDO. The mixture was poured into the chaotic mixer preheated at 110°C and mixed for 5 min. Approximately 70 cm^3 of TPU or its composite was prepared in one batch in the chaotic mixer. The materials were mixed in the chaotic mixer using circular rotors corotating in a sinusoidal fashion at the peak speed of 65 rpm, which generated a peak shear rate of 9.5 and 5.4 s^{-1} at the rotors surface and at the mixing chamber walls respectively. The time-averaged mean shear rate in

the mixer was 3.8 s^{-1}. The use of circular rotors and low mean shear rate of 3.8 s^{-1} produced uniform mixing of the ingredients without appreciable fiber breakage [39, 40]. Additional details on the chaotic mixer used in this study can be found elsewhere [41]. The composite materials collected from the mixer were compression molded at 220°C for 1 min; the total time elapsed in preheating the materials from room temperature, degassing, and compression molding was 7 min.

Characterization

Electrical Volume Conductivity. Compressed sheets of composite materials were placed in a Keithley 8009 Resistivity Test Chamber (Cleveland, OH) for electrical conductivity measurements according to ASTM D 257 method using Keithley 487 picoammeter/voltage source (Cleveland, OH). A maximum error of 10% was incurred in these measurements as revealed from at least five readings taken on each specimen.

Thermal Properties. Thermal properties such as glass transition temperature (T_g) and hard segment melting point (T_m) of TPU and composites were determined using a TA Instruments 2920 Modulated DSC (New Castle, DE) at a heating rate of 10°C/min in the range of −100 to 230°C. Specimens weighing 3.8 mg were heated from −100 to 100°C at 10°C/min to determine soft segment crystallinity. The heat of fusion was obtained from DSC traces of second thermal scans. The percent crystallinity was determined by comparing the heat of fusion of soft segment crystals with the heat of fusion of 100% crystalline PCL-diol—136 J/g [32]. The crystallinity data were also verified using cooling scans performed from 100°C down to −30°C at 10°C/min.

Dynamic Mechanical Analysis. Dynamic mechanical analysis (DMA) was performed with a Pyris Diamond DMA, from Perkin Elmer-Seiko Instruments (Boston, MA) in tensile mode at 3°C/min under nitrogen atmosphere, 1 Hz frequency, and thermal scans from −90 to 40°C.

Infrared Spectroscopy. The extent of hydrogen bonding in TPU and its composites was determined using infrared spectroscopy. The hydrogen bonding index, R, was determined from the ratio of areas of deconvoluted peaks corresponding to hydrogen-bonded (∼1700 cm^{-1}) and free (∼1730 cm^{-1}) carbonyl groups that appeared in infrared spectrum of TPU. Films of TPU were cast on KBr disc from a solution in dimethylformamide, and FTIR spectra were recorded at room temperature from 4000 to 800 cm^{-1} with a Perkin Elmer 16 PC FTIR (Wellesley, MA) in transmission mode and 4 cm^{-1} resolution. FTIR spectra were also recorded after placing TPU films on a hot stage and heating the specimens up to 60, 120, and 180°C at ∼20°C/min heating rate. A deconvolution software was applied to determine the ratio of area under N—H (A_{NH}) and C—H (A_{CH}) peaks as a function of temperature. In all cases, the data were accepted only after the difference between the original spectra and simulated spectra came close to zero.

Tensile Properties. Tensile properties of composites were evaluated according to ASTM D-638 method by means of Instron 5567 tensile tester (Norwood, MA) with a crosshead speed of 100 mm/min, gauge length of 20 mm, strain rate of 0.083 s^{-1}, and a load cell of 100 N.

Morphological Analysis. Morphology of composites was analyzed using optical microscopy and scanning electron microscopy (SEM). Leitz Laborlux 12 Pol S (Oberkochen, Germany) optical microscope fitted with a Diagnostic Instruments 11.2 Color Mosaic digital camera (Sterling Heights, MI) was used in transmission mode to record CNF dispersion in 100-μm thin samples. SEM images of fractured specimens were taken using a SEM S-2150 from Hitachi (Ibaraki, Japan) at 20 kV. Samples were coated with silver using a K575x sputter coater from Emitech (Kent, England) under argon gas atmosphere.

Shape-Memory Properties. Rectangular strips of dimension 50 × 5 × 0.5 mm^3 were cut out of the compressed polymer specimens. Strips with 20-mm gauge length (L_0) were clamped on Instron 4204 Tensile Tester adapted with a heating chamber, and the temperature was slowly raised to 60°C. The upper grip of the tensile tester was moved at 20 mm/min to reach a predetermined extended length (L_1) to give 100% strain to the specimen. The specimen with tensile load in place was cooled with an electric fan; in ∼30 s, the temperature dropped to 40°C, below the melting point of the PCL-diol crystals. The specimen was then allowed to cool to room temperature (25°C) in ∼9 min and the tensile load was removed. The new specimen length L_2 was measured, and the percentage of shape retention or fixity was determined from the following equation:

$$\text{Shape fixity } (\%) = \frac{(L_2 - L_0)}{(L_1 - L_0)} \times 100 \qquad (1)$$

An elongated specimen of length L_2 produced as mentioned earlier was placed in a Pyris Diamond DMA apparatus and heated at 4°C/min from room temperature to 100°C. The specimen would undergo shape recovery under this condition. However, its length was held constant at L_2, and the force needed to maintain the length was measured as a function of temperature. This force was later reported as the shape recovery force of the specimen.

Shape recovery by Joule heating was also investigated in this work. The initial deformed state was produced by

 DOI 10.1002/pen

bending a strip of rectangular specimen (length, width, and thickness, respectively, 34 mm, 15 mm, and 0.46 mm) at halfway mark along the length. For this purpose, a strip of electrically conductive composite material was placed in an oven at 80°C for 5 min for melting of the soft segment crystals, quickly deformed inside the oven by folding at halfway mark along the length, and cooled in ice–water mixture to retain the deformed shape. The deformed specimen produced an angle θ of $\sim 38^\circ$ with the vertical. The specimen was then clamped along the width between the alligator clips of electrodes, and a desired voltage was applied to affect shape recovery. The change in the value of θ was recorded by means of a video camera, and the surface temperature of the specimen was recorded with an accuracy of $\pm 5^\circ$C by means of an IR sensor gun pointing at the midpoint of the part of the strip undergoing shape recovery. The accuracy of the IR sensor gun was previously checked against a standard thermocouple by simultaneously measuring the temperature of the same composite specimen.

RESULTS AND DISCUSSION

State of Carbon Nanofibers Dispersion

Our previous study [40] showed that the presence of oxygen-rich polar functional groups on the surfaces of ox-CNF promoted better wetting by TPU and produced better dispersion of ox-CNF than CNF in TPU. It was learned from the areas under the peaks assigned to C(1s) and O(1s) in XPS spectra that ox-CNF contained ~ 10 times more surface oxygen than CNF [40]. Figure 1 presents optical micrographs of compressed films of composites containing 1 wt% CNF (Fig. 1a) and 1 wt% ox-CNF (Fig. 1b) and reveals that ox-CNF bundles were much better dispersed than those of CNF as observed in an earlier study [40]. Similar behavior can be observed through the SEM photos presented in Fig. 2 for 5 wt% respective composites. In this context, note that mixing in the chaotic mixer was primarily of distributive type—the rotors of circular cross-section produced distributive mixing and the mean shear rate was low, $\sim 4\ s^{-1}$. Better dispersion of ox-CNF particles seen in Figs. 1b and 2b also presented the possibility of stronger interactions between the polar functional groups on ox-CNF surfaces, mainly the carbonyls, and the TPU.

The amounts of hard segment domains formed by the urethane linkages can be estimated from the area under the peak of hydrogen-bonded (A_{HCO}; at 1701 cm^{-1}) and free carbonyl groups (A_{CO}; at 1725 cm^{-1}) [42, 43]. However, in this study, the PCL-diol soft segments also contributed carbonyl groups. In view of this, the ratio A_{HCO}/A_{CO} was used as a measure of the extent of hydrogen-bonded carbonyl groups in TPU and its composites. In addition, the extent of hydrogen-bonded —NH— groups was determined from the ratio of A_{NH}/A_{CH}, where A_{NH} is the area under the —NH— groups in urethane linkages and A_{CH} is the area under the peak for —CH— stretching. The ratio A_{NH}/A_{CH} was used to monitor the thermal stability of hydrogen bonds formed by the

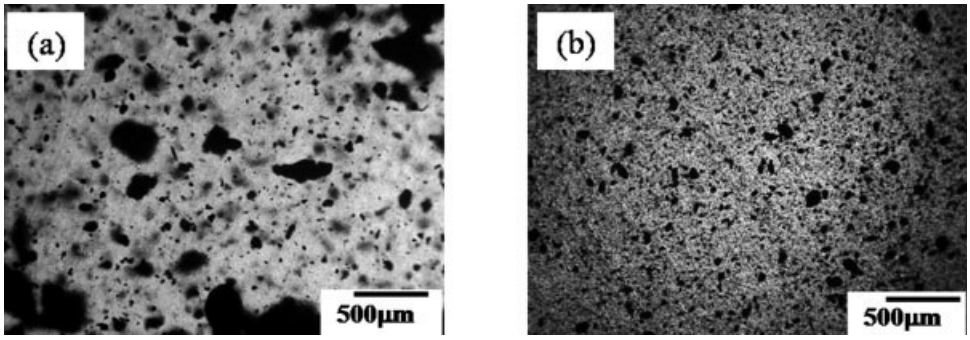

FIG. 1. Optical micrographs of TPU composites with 1 wt% of (a) CNF and (b) ox-CNF.

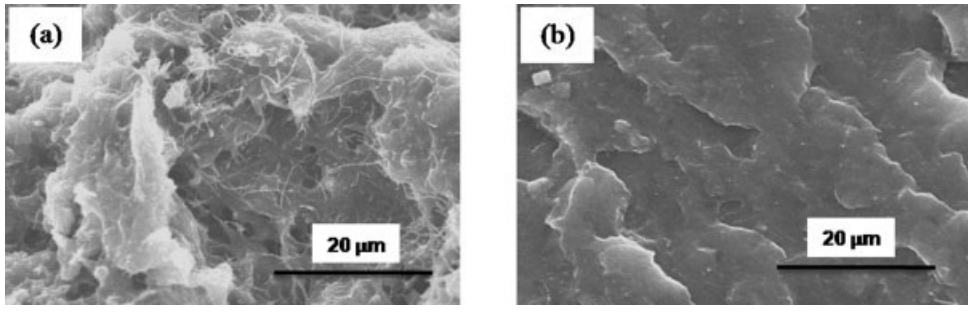

FIG. 2. SEM micrographs of composites with 5 wt% (a) CNF and (b) ox-CNF.

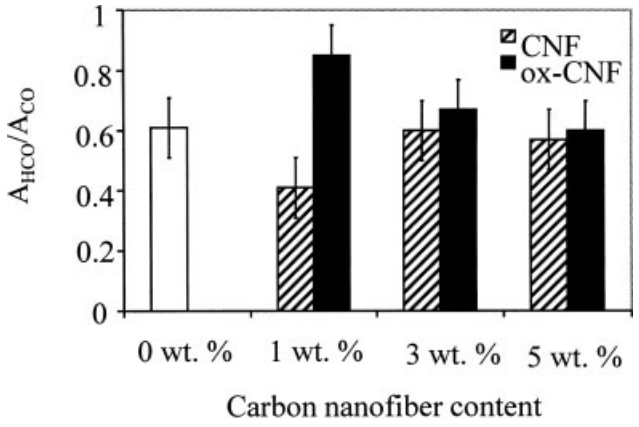

FIG. 3. The values of A_{HCO}/A_{CO} for various composite specimens. The error bars represent errors originating from fitting of FTIR spectra. These were obtained by repeating fitting of experimental FTIR spectra for each specimen at least three times.

urethane linkages in the presence of CNF. The —NH— groups in urethane linkages are identified by four overlapping symmetric peaks at 3440, 3320, 3270, and 3180 cm^{-1} and are assigned to free —NH—, hydrogen-bonded —NH—, trans, and cis —NH— conformations, respectively [44]. The hydrogen in —NH— groups in the hard segments can interact with other functional groups, namely carbonyl groups either in the hard or in the soft segments, and even with π-electrons of the aromatic rings [45]. The values of A_{HCO}/A_{CO} for various composites at room temperature are shown in Fig. 3. As a general trend, the amounts of hydrogen-bonded carbonyl groups reduced in the presence of CNF, whereas it increased in composites of ox-CNF. This can be attributed to physical interference of CNF with the TPU hard segments. The additional hydrogen-bonded carbonyls in the case of ox-CNF may have originated from the interaction of —NH— groups in the hard segments with the carbonyl groups present on the surface of ox-CNF [40].

The thermal stability of hydrogen-bonded —NH— groups was studied to determine the influence of CNFs on thermal stability of hard segments, especially in light of several heating and cooling cycles that shape-memory materials would experience. In this work, the thermal stability of hydrogen-bonded —NH— groups in TPU and its composite with 7 wt% CNF was analyzed. The specimens were heated to prescribed temperatures with a heating rate of 20°C/min, and the values of A_{NH}/A_{CH} ratio were determined (Table 1). It is noticed that the extent of hydrogen-bonded NH groups reduced with an increase in temperature especially at temperatures of 120°C and above, which can be related to the glass transition of the hard segments [44]. It is important to note that even at 180°C, some hydrogen-bonded —NH— groups survived. It was reported previously that significant hydrogen bonding can survive at even 200°C in TPU [44]. The reduction of A_{NH}/A_{CH} values with the increase of temperature in Table 1 seems to be more rapid for the composite than

TABLE 1. Effect of temperature on the values of A_{NH}/A_{CH} in TPU and its composite with 7 wt% CNF.

Temperature (°C)	A_{NH}/A_{CH} for TPU	A_{NH}/A_{CH} for composite of 7 wt% CNF
25	0.40	0.39
60	0.42	0.35
120	0.28	0.30
180	0.25	0.28

The specimens were heated to prescribed temperatures at 20°C/min.

for the neat polymer in the range from 25 to 60°C. One reason for this behavior might be the ability of the CNFs to improve the thermal conductivity of the polymer, thus allowing for more uniform heating and disruption of the hydrogen bonds in the composites at 60°C and above than in TPU. Note that solution cast specimens used to obtain FTIR data were thin and the heating rate was 20°C/min. Such effect was also reflected in the reduction of hydrogen-bonded carbonyl groups, as seen in Fig. 4. It is observed in Fig. 4 that the hydrogen-bonded CO groups remained almost intact at 60°C in the case of neat TPU

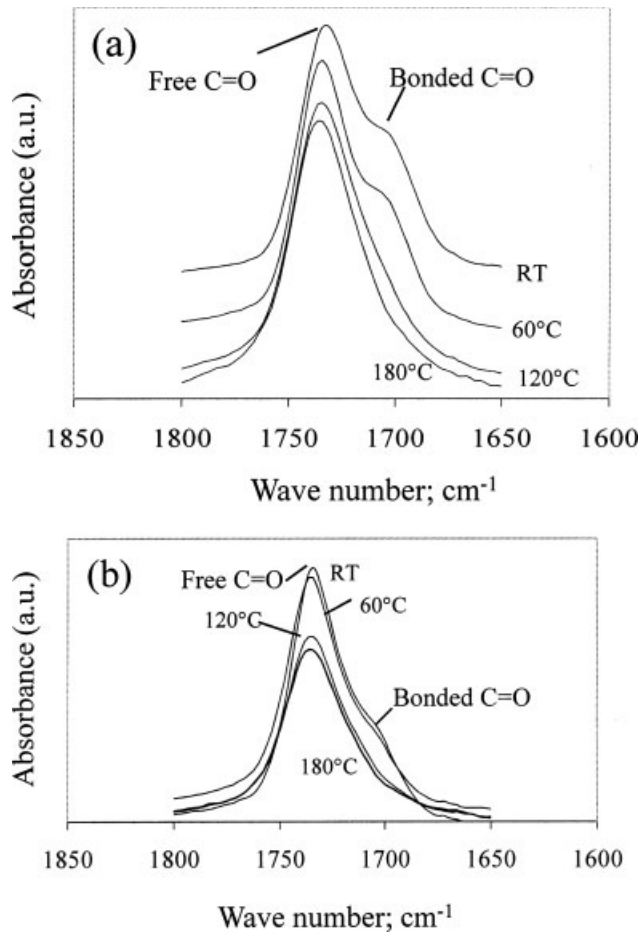

FIG. 4. FTIR spectra of C=O stretching region at different temperatures for (a) TPU and (b) composite of 7 wt% CNF. RT stands for room temperature (25°C).

DOI 10.1002/pen

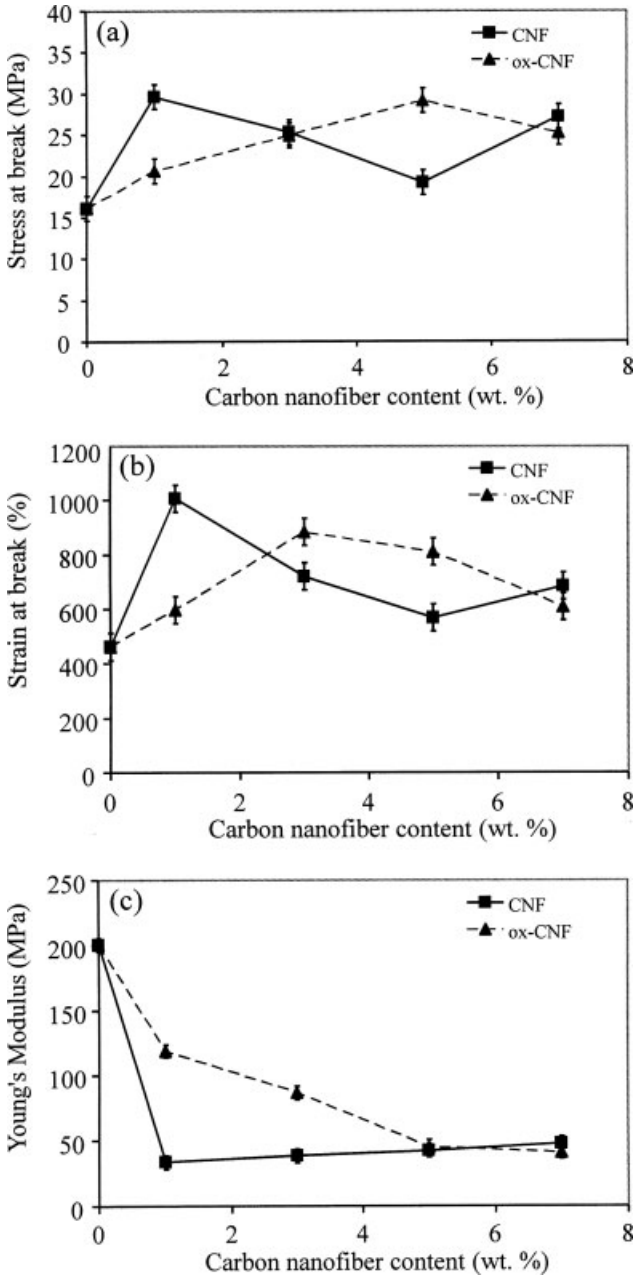

FIG. 5. Tensile properties of CNF and ox-CNF composites at room temperature: (a) stress at break, (b) strain at break, and (c) Young's modulus.

(Fig. 4a) and its composites (Fig. 4b), whereas they turned into free CO groups at 120°C. In view of the data presented in Fig. 4 and Table 1, one can suggest that hydrogen-bonded —NH— and carbonyl groups remained intact at 60°C, the temperature at which the specimens for testing of shape-memory properties were prepared.

Mechanical and Thermomechanical Properties

Tensile strength and strain and Young's modulus of CNF and ox-CNF composites at room temperature are presented in Fig. 5. In general, the values of tensile stress and strain increased in the presence of nanofibers. The tensile stress and strain increased, respectively, ~100 and 150% over TPU in the presence of 1 wt% CNF. At higher CNF loading, however, the tensile stress and strain reduced apparently because of an increase in the number and size of CNF agglomerates. On the other hand, the tensile stress at break increased up to 5 wt% ox-CNF; this can be attributed to better nanofiber dispersion [40]. The Young's modulus showed a drop with the addition of either CNF or ox-CNF (Fig. 5c), although greater reduction was observed in the case of CNF. This can be attributed to several factors, for example, reduction in soft segment crystallinity [28, 30], incomplete wetting of nanofiber bundles by the polymer [46], and attrition of fiber aspect ratio [39]. Recent studies elucidated that full potential for reinforcement by individual nanoparticles is compromised if they are present as fractal aggregates or as bundles [47, 48] and that better reinforcement is obtained when the particles are dispersed to nanoscale.

The soft segment crystallinity of the composites was evaluated using DSC (see Fig. 6). The composite specimens were subjected to two consecutive heating scans to unravel the influence of CNFs on soft segment crystallinity. The crystallinity of PCL-diol soft phase was evaluated from the ratio of the heat of fusion of each melting endotherm and the heat of fusion of a 100% crystalline PCL-diol [32]. In general, PCL-diol crystallinity in composites reduced in the presence of either CNF or ox-CNF. Such reduction was less dramatic in the case of composites of ox-CNF. A higher crystallinity in second thermal scan in

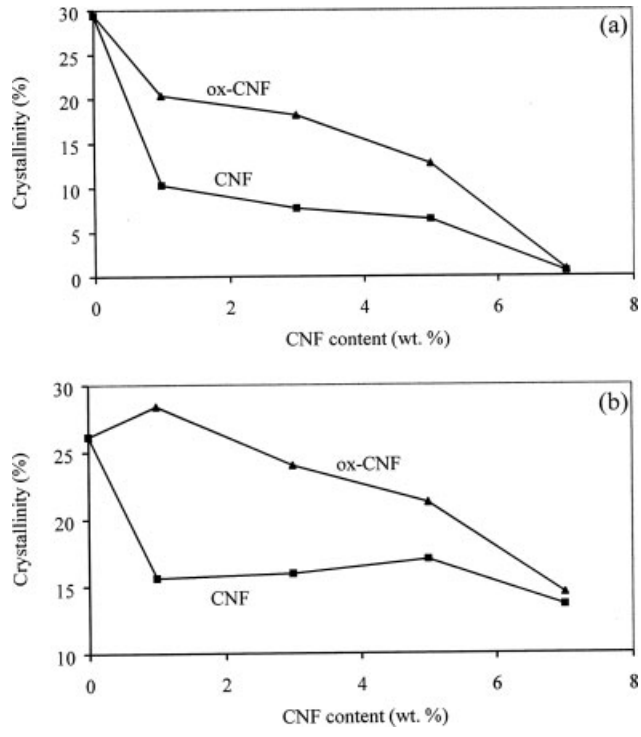

FIG. 6. Soft segment crystallinity of composites (a) first and (b) second thermal scan in DSC.

the presence of 1 wt% ox-CNF (Fig. 6b) can be attributed to nucleation of PCL-diol crystals. Other investigators also reported nucleation in TPU in the presence of CNF [34], SWNT [49], and nanoclay [50], although Cao and Jana [28] reported 26% reduction in PCL-diol crystallinity in the presence of 5 wt% organically modified layered silicate clay. Gunes et al. [30] reported dramatic reduction of soft segment crystallinity in the presence of CNF, CB, and silicon carbide nanoparticles when the composites were prepared in a commercial internal mixer.

To elucidate the effects of reinforcement by CNF and ox-CNF nanofibers without consideration of PCL-diol crystals, the tensile properties were evaluated at 60°C. This also allowed us to estimate the reinforcement effect of the hard microdomains [32]. Figure 7 shows the values of maximum stress and Young's modulus when TPU composite specimens were stretched by 100% at 60°C. Note that the tensile properties in this case relied only on the hard segment domains and the reinforcement effect of CNF or ox-CNF as PCL-diol crystals were all melted. It was observed that pristine TPU could be stretched only up to 76% at 60°C, whereas specimens of CNF and ox-CNF composites could be easily stretched to 100% of their length. In view of this, the values of stress at 100 and 76% strain, respectively, for composites and neat TPU were taken into account for comparison. The maximum stress increased with CNFs content. In light of the data provided in Figs. 6 and 7, it can be inferred that the modulus of composites at room temperature was largely

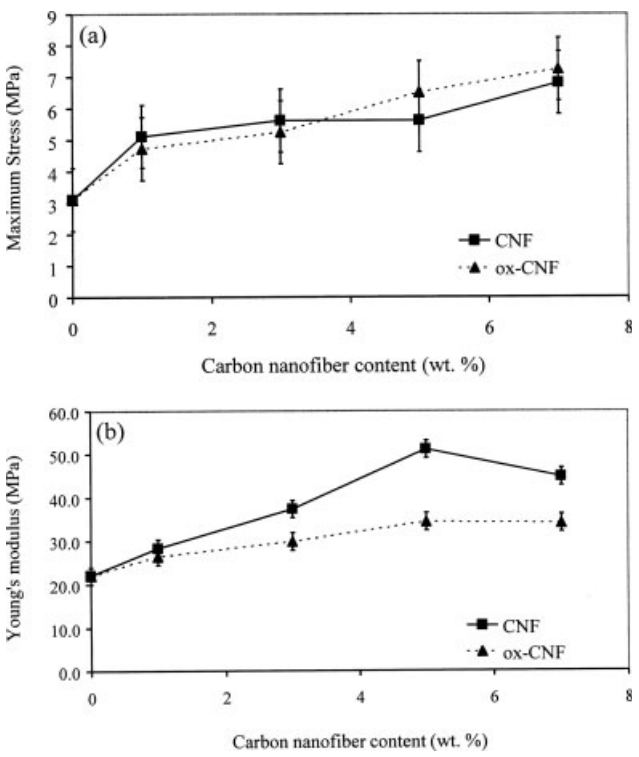

FIG. 7. Tensile properties at 60°C and 100% strain for CNF and ox-CNF composites. (a) Maximum stress and (b) Young's modulus.

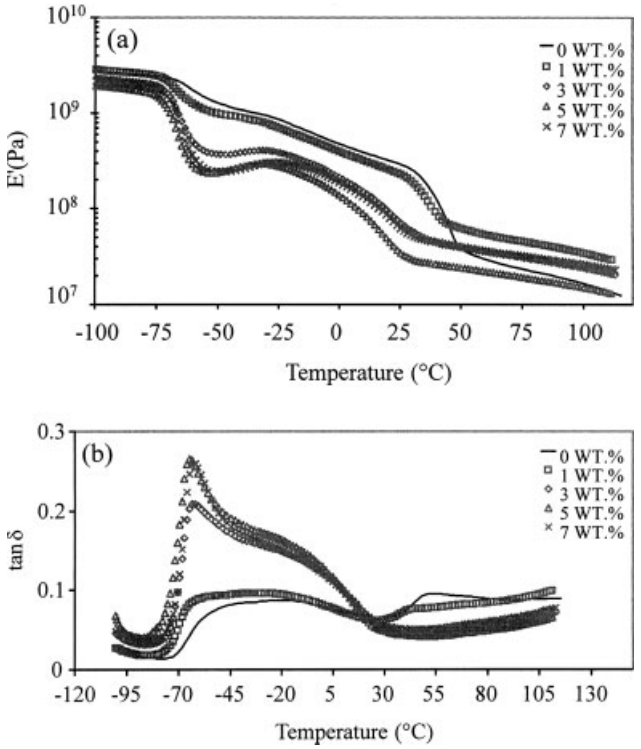

FIG. 8. Thermomechanical properties of CNF composites: (a) storage modulus and (b) tan δ.

determined by the extent of PCL-diol crystals as reported previously for composites of nanoclay [28] and silicon carbide and CB [30]. In this work, the formation of PCL-diol crystals in composites was impeded at room temperature because of the presence of CNFs, thus causing a reduction of the values of Young's modulus for CNF and ox-CNF composites. However, once the crystals were melted, e.g., at 60°C, reinforcement by nanofibers became noticeable.

Similar trends were observed in dynamic mechanical properties of CNF and ox-CNF composites as presented in Figs. 8 and 9. The values of storage modulus, E', (Figs. 8a and 9a) show slightly lower glassy plateau modulus for the composites compared with TPU. This corresponds to the reduction in the PCL crystallinity, as discussed previously. A drop in the values of E' versus temperature represents the onset of the glass transition, which was more prominent for CNF composites with content above 1 wt%, as seen in Fig. 8a, and above 3 wt% ox-CNF, as in Fig. 9a. In general, all the composites experienced a decline in the values of E' between 25 and 50°C, because of the melting of the PCL crystals. The reinforcement effect produced by the nanofibers became apparent above 50°C as the composites showed higher E' values than pristine TPU.

The glass transition behavior can be analyzed from the tan δ vs. temperature plots in Figs. 8b and 9b. The glass transition for pristine TPU was broad and showed low tan δ values, indicating that less amorphous polymer

 DOI 10.1002/pen

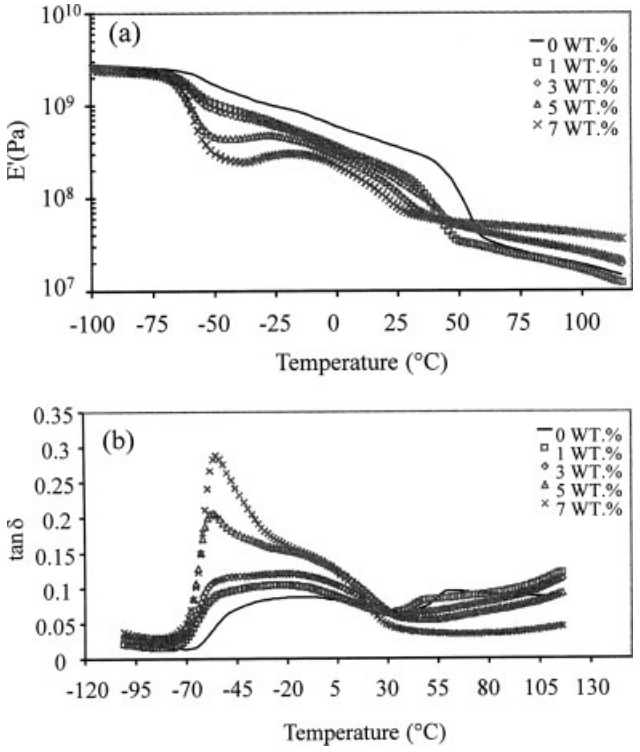

FIG. 9. Thermomechanical properties of ox-CNF composites: (a) storage modulus and (b) tan δ.

chains participated in glass transition and that PCL-diol crystallinity was higher. However, the amounts of amorphous chains in composites of CNF increased beyond 1 wt% of nanofiber content as reflected from higher values of tan δ. In contrast, the composites of ox-CNF did not show a well-defined glass transition peak up to 3 wt% ox-CNF (Fig. 9b).

Shape-Memory Properties

Gunes et al. [30] reported the effects of CNF, silicon carbide, CB, and layered silicate clay on shape-memory properties of TPU composites prepared in Brabender Plasticorder® batch mixer. It was found that shape fixity of composites of CNF showed dramatic reduction, e.g., 49, 41, and 31%, respectively, in the presence of 1, 3, and 5 wt% CNF compared with 93% for unfilled TPU when stretched to 100% of original lengths. This was attributed to reduction in soft segment crystallinity of PCL-diol from ~29% for unfilled TPU to less than 2% in the presence of CNF. It was noted by Jimenez and Jana [39, 40] that CNF particles underwent severe attrition of lengths when composites were prepared in Brabender Plasticorder batch mixer, whereas the composites prepared under similar conditions of shear rate in the chaotic mixer preserved fiber aspect ratio. The composites prepared in this study also showed a reduction of shape fixity in the presence of CNFs (see Fig. 10). However, the reduction is more severe in the case of CNF composites, e.g., the shape fixity reduced from ~90% for unfilled TPU to less than 20% in the presence of 1 wt% CNF. On the other hand, shape fixity decreased gradually with ox-CNF content, e.g., ~70% with 1 wt% ox-CNF and ~50% with 3 wt% ox-CNF.

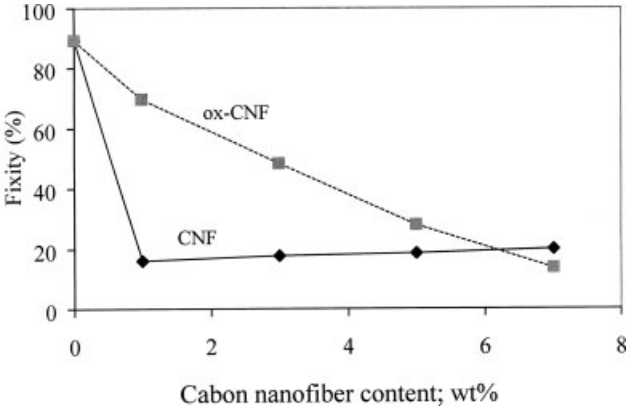

FIG. 10. Shape fixity of composites subjected to 50% strain at 60°C.

Figure 11 presents the values of recovery stress in composite specimens that were initially elongated to 100% of original lengths at 60°C. In some cases, the specimens became soft at higher temperature and broke, e.g., at 5 wt% in Fig. 11a and 1 wt% in Fig. 11b. Consequently, DMA stopped sensing the mechanical resistance of these materials. It is seen that the recovery stress assumed maximum values in the neighborhood of the

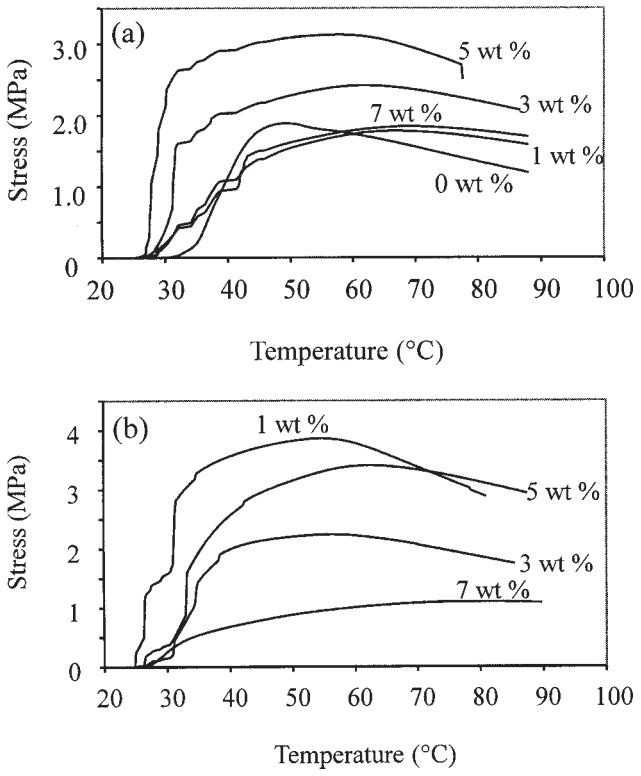

FIG. 11. Recovery stress in composites of (a) CNF and (b) ox-CNF.

deformation temperature (in this case 60°C) as reported by other researchers [37]. The data in Fig. 11 show that highest recovery stress, respectively, 3 and 4 MPa, was seen for composites of 5 wt% CNF (Fig. 11a) and 1 wt% ox-CNF (Fig. 11b); these values are much higher than the recovery stress of ~1.8 MPa for unfilled TPU. In general, the composites with 7 wt% of CNFs showed the lowest recovery stress among the materials tested. Cao and Jana [28] attributed lower recovery stress at higher nanoclay content in to faster stress relaxation during stretching and cooling of specimens. Similar phenomenon may have taken place in this study as well. Nevertheless, the values of recovery stress reported in Fig. 11 are similar to those reported by other investigators. For example, Kim et al. [19] reported recovery stress ~2.5 MPa for TPU synthesized from PCL-diol of molecular weight 4000, MDI, and BDO with 30 wt% hard segments. Koerner et al. [33] reported a recovery stress of 1.5 MPa for polyurethanes containing 5 wt% of heat-treated CNF. Recently, Mondal and Hu [51] observed a maximum recovery stress of 1 MPa in polyether-based TPU composite of 1.5 wt% functionalized MWNT.

Only two composite specimens—with 5 and 7 wt% CNF—prepared in the chaotic mixer showed low enough surface electrical resistivity, 2.67×10^7 and 2.46×10^7 ohm, respectively (Table 2). Gunes et al. [52] reported that composites of CNF and ox-CNF did not show positive temperature coefficient effects because of low levels of soft segment crystallinity and, therefore, resistive heating was possible even when all PCL-diol crystals were melted. Also, the strains due to thermal expansion in these composites were order of magnitude smaller than shape recovery strain, and thus the conductive networks survived at higher temperature [29]. This aided the demonstration of shape-memory actions actuated by resistive heating. Figure 12 shows how the temperature changed during application of voltage on these two composite specimens. It is seen that Joule heating was more important for the composite with 5 wt% CNF, e.g., at 300 V (Fig. 12a) compared with the composite of 7 wt% CNF (Fig. 12b). The surface temperature of composite specimen with 5 wt% CNF reached a value greater than 50°C with the application of voltage of 300 V for greater than 45 s. Cho and coworkers [36, 37] observed a temperature increase of 35°C in 8 s by exposing a composite of TPU with 5 wt% of acid-treated MWNT to an applied voltage of 60 V. The amount of heat generated, Q in time t, depends on the resistance, R, of the material and the electrical current, I, according to *Eq. 2*.

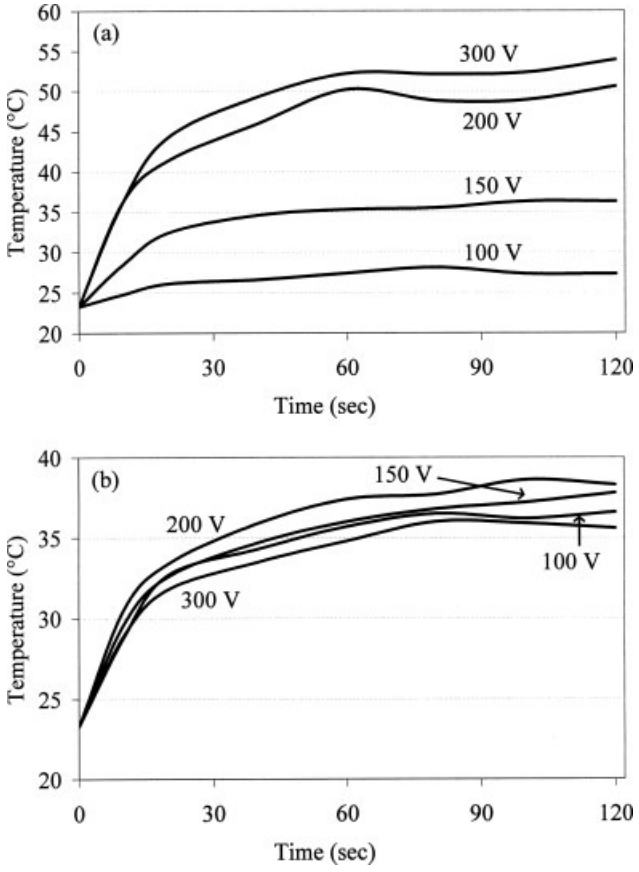

FIG. 12. Increase of temperature with applied voltage for (a) TPU/CNF 5 wt% and (b) TPU/CNF 7 wt% composites. Electrical conductivity values are presented in Table 2.

$$Q = RI^2t \tag{2}$$

Although Joule heating requires higher electrical resistivity (R), it depends on the square of the electrical current. It was found that composites of ox-CNF did not produce Joule heating for applied voltages between 100 and 300 V because of much higher resistivity (Table 2) and

TABLE 2. Surface resistivity and volume electrical conductivity of TPU composites at room temperature.

Nanofiber content (wt%)	Applied voltage (V)	Surface resistivity (ohm)		Volume conductivity (S/cm)	
		CNF	ox-CNF	CNF	ox-CNF
0	500	3.74×10^{14}	3.74×10^{14}	1.86×10^{-13}	1.86×10^{-13}
1	500	8.54×10^{13}	1.92×10^{14}	2.25×10^{-13}	3.06×10^{-12}
3	1	1.17×10^{11}	2.30×10^{14}	9.28×10^{-8}	5.72×10^{-13}
5	1	2.67×10^{7}	6.41×10^{11}	1.86×10^{-5}	4.16×10^{-6}
7	1	2.46×10^{7}	1.71×10^{9}	1.77×10^{-5}	8.96×10^{-6}

A maximum error of 10% was incurred in these measurements as revealed from least five readings taken on each specimen.

 DOI 10.1002/pen

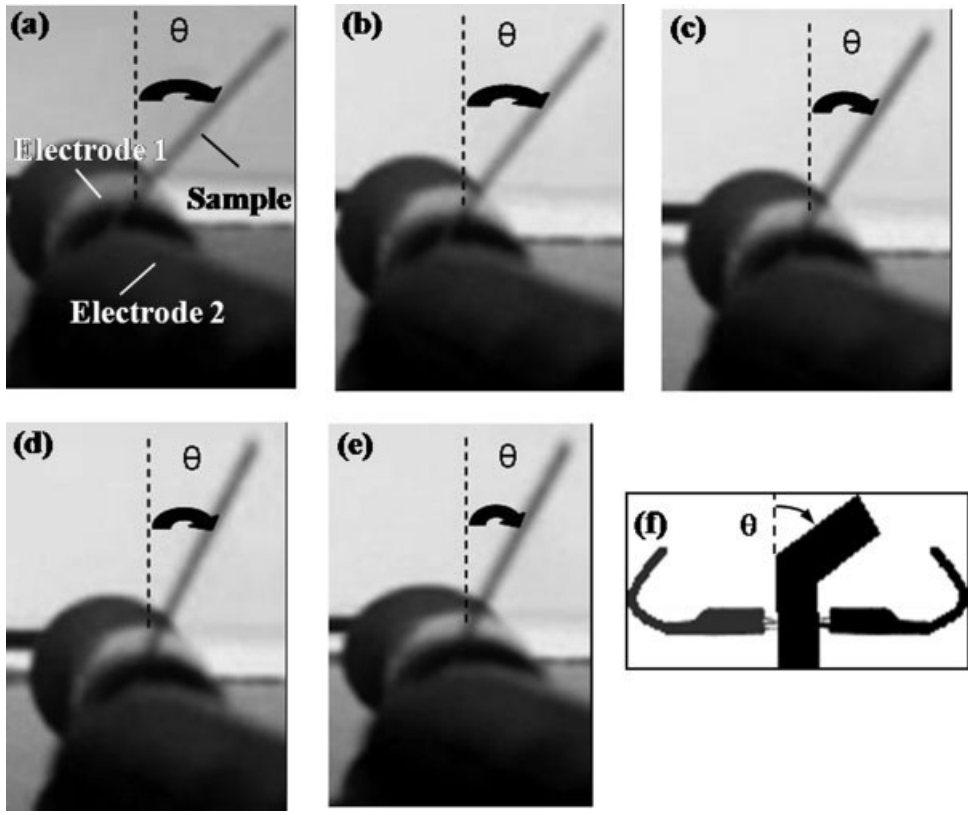

FIG. 13. Shape recovery of TPU/5 wt% CNF composite triggered by Joule heating after application of 300 V: (a) 0 s, (b) 10 s, (c) 20 s, (d) 40 s, (e) 60 s, and (f) schematic representation of the electrode setup.

hence lower current density. The shape recovery of composite specimens by Joule heating was observed by recording the images of deformed specimen using a video camera. The image frames were captured at time intervals of 10 s as shown in Fig. 13. It can be appreciated from Fig. 13 that the deformed specimen began shape recovery and the angle θ of the bent specimen with respect to an imaginary vertical line began to reduce after 20 s of application of the electrical voltage (300 V). Such recovery stopped after $\sim$60 s of application of voltage and the value of θ reached a constant value (see Fig. 14).

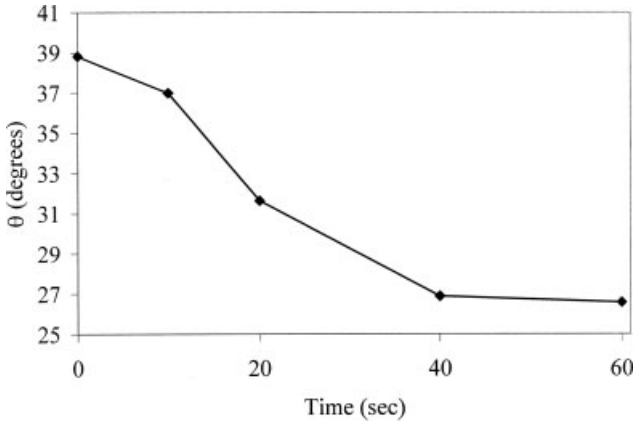

FIG. 14. Change of the angle of deformation, θ, with time in a specimen of composite of 5 wt% CNF. Straight lines are used to guide the eye.

CONCLUSIONS

The study showed that better dispersion ox-CNF in TPU produced under low shear chaotic mixing conditions gave rise to better shape-memory properties than with CNF particles. It was also seen that PCL-diol crystals played important role in producing electrically conductive composites. The surface resistivity of these conductive composites was enough to trigger shape recovery by resistive heating. In general, it was found that CNFs interacted with both the hard and the soft segment in TPU, and such interaction was detrimental to the crystallinity of the soft phase and to the hydrogen bonding inside the microcrystalline hard segment domains. It was also seen that the crystallizable soft segments in TPU controlled the mechanical properties at room temperature. It became clear that both PCL-diol crystallinity and the presence of CNFs play an important role in determining the percentage of fixity and recovery stress in thermally actuated shape-memory behavior.

REFERENCES

1. D. Randall, S. Lee, and G. Woods, *The Polyurethanes Book*, Wiley, New York (2002).

2. N.M.K. Lamba, K.A. Woodhouse, S.L. Cooper, and M.D. Lelah, *Polyurethanes in Biomedical Applications*, CRC Press, Florida (1998).
3. G.M. Estes, R.W. Seymour, and S.L. Cooper, *Macromolecules*, **25**, 452 (1971).
4. R. Bonart, *J. Macromol. Sci. Phys. B*, **2**, 115 (1968).
5. C.E. Wilkes and C.S.J. Yusek, *Macromol. Sci. Phys. B*, **7**, 157 (1973).
6. J.L. Blackwell and K.H. Gardner, *Polymer*, **20**, 13 (1979).
7. J.L. Blackwell and C.D. Lee, *J. Polym. Sci. Polym. Phys. Ed.*, **21**, 2169 (1983).
8. A. Lendlein and S. Kelch, *Angew. Chem. Int. Ed. Engl.*, **41**, 2034 (2002).
9. V.A. Beloshenko, V.N. Varyukhin, and Y.V. Voznyak, *Russ. Chem. Rev.*, **74**, 265 (2005).
10. C. Liu, H. Qin, and P.T. Mather, *J. Mater. Chem.*, **17**, 1543 (2007).
11. I.S. Gunes and S.C. Jana, *J. Nanosci. Nanotechnol.*, **8**, 1616 (2008).
12. G.R. Nelson, U.S. Patent 3,284,275 (1966).
13. S. Hayashi and H. Fujimura, U.S. Patent 5,049,591 (1991).
14. S. Hayashi, H. Fujimura, and M. Shimizu, U.S. Patent 5,139,832 (1992).
15. S. Hayashi, U.S. Patent 5,145,935 (1992).
16. S. Hayashi, *Int. Prog. Urethanes*, **6**, 90 (1993).
17. S. Hayashi, S. Kondo, P. Kapadia, and E. Ushioda, *Plast. Eng.*, **51**, 29 (1995).
18. B.S. Lee, B.C. Chun, Y.C. Chung, K.I. Sul, and J.W. Cho, *Macromolecules*, **34**, 6431 (2001).
19. B.K. Kim, S.Y. Lee, and M. Xu, *Polymer*, **37**, 5781 (1996).
20. T. Takahashi, N. Hayashi, and S. Hayashi, *J. Appl. Polym. Sci.*, **60**, 1061 (1996).
21. F.K. Li, X. Zhang, J.N. Hou, M. Xu, X.L. Lu, D.Z. Ma, and B.K. Kim, *J. Appl. Polym. Sci.*, **64**, 1511 (1997).
22. C. Liang, C.A. Rogers, and E.J. Malafeew, *Intell. Mater. Syst. Struct.*, **8**, 380 (1997).
23. J.R. Lin and L.W. Chen, *J. Appl. Polym. Sci.*, **69**, 1563 (1998).
24. J.R. Lin and L.W. Chen, *J. Appl. Polym. Sci.*, **69**, 1575 (1998).
25. J.R. Lin and L.W. Chen, *J. Appl. Polym. Sci.*, **73**, 1305 (1999).
26. P. Ping, W.S. Wang, X.S. Chen, and X.B. Jing, *Biomacromolecules*, **6**, 587 (2005).
27. H.M. Jeong, J.B. Lee, S.Y. Lee, and B.K. Kim, *J. Mater. Sci.*, **35**, 279 (2000).
28. F. Cao and S.C. Jana, *Polymer*, **48**, 3790 (2007).
29. I.S. Gunes, F. Cao, and S.C. Jana, *J. Polym. Sci. Part B: Polym. Phys.*, **46**, 1437 (2008).
30. I.S. Gunes, F. Cao, G. Jimenez, and S.C. Jana, *Polymer*, **49**, 2223 (2008).
31. F.K. Li, J.N. Hou, W. Zhu, X. Zhang, M. Xu, X.L. Luo, D.Z. Ma, and B.K. Kim, *J. Appl. Polym. Sci.*, **62**, 631 (1996).
32. F.K. Li, L.Y. Qi, J.P. Yang, M. Xu, X.L. Luo, and D.Z. Ma, *J. Appl. Polym. Sci.*, **75**, 68 (2000).
33. H. Koerner, G. Price, N.A. Pearce, M. Alexander, and R.A. Vaia, *Nat. Mater.*, **3**, 115 (2004).
34. H. Koerner, W. Liu, M. Alexander, P. Mirau, H. Dowty, and R.A. Vaia, *Polymer*, **46**, 4405 (2005).
35. I.H. Paik, N.S. Goo, Y.C. Jung, and J.W. Cho, *Smart Mater. Struct.*, **15**, 1476 (2006).
36. J.W. Cho, J.W. Kim, Y.C. Jung, and N.S. Goo, *Macromol. Rapid Commun.*, **26**, 412 (2005).
37. H.J. Yoo, Y.C. Jung, N.G. Sahoo, and J.W. Cho, *J. Macromol. Sci. Phys.*, **45**, 441 (2006).
38. B.A. Higgins, "Carbon Nanofiber-Polymer Composites for Electronic Applications," Ph.D. Thesis, University of Akron, OH (2006).
39. G.A. Jimenez and S.C. Jana, *Compos. Part A: Appl. Sci. Manuf.*, **38**, 983 (2007).
40. G.A. Jimenez and S.C. Jana, *Carbon*, **45**, 2079 (2007).
41. C.D. Jung, I.S. Gunes, and S.C. Jana, *Ind. Eng. Chem. Res.*, **46**, 2413 (2007).
42. H.S. Lee, Y.K. Wang, W.J. Macknight, and S.L. Hsu, *Macromolecules*, **21**, 270 (1988).
43. M.M. Coleman, K.H. Lee, D.J. Skrovanek, and P.C. Painter, *Macromolecules*, **19**, 2149 (1986).
44. V.W. Srichatrapimuk and S.L. Cooper, *J. Macromol. Sci. Phys. B*, **15**, 267 (1978).
45. F.C. Wang, M. Feve, T.M. Lam, and J.P. Pascault, *J. Polym. Sci. Part B: Polym. Phys.*, **32**, 1305 (1994).
46. G.G. Tibbetts, I.C. Finegan, and C. Kwag, *Mol. Cryst. Liq. Cryst.*, **387**, 129 (2002).
47. D.W. Schafer and R.S. Justice, *Macromolecules*, **40**, 8501 (2007).
48. T.A. Witten, M. Rubinstein, and R.H. Colby, *J. Phys. II (France)*, **3**, 367 (1993).
49. H.S. Xia and M. Song, *J. Mater. Chem.*, **16**, 1843 (2006).
50. M. Tortora, G. Gorrasi, V. Vittoria, G. Galli, S. Ritrovati, and E. Chiellini, *Polymer*, **43**, 6147 (2002).
51. S. Mondal and J.L. Hu, *J. Elast. Plast.*, **38**, 261 (2006).
52. I.S. Gunes, G. Jimenez, and S.C. Jana, *Carbon*, **47**, 981 (2009).

 DOI 10.1002/pen